PCCP

Accepted Manuscript

ROYAL SOCIETY OF CHEMISTRY

www.rsc.org/pccp

Journal Name

ARTICLE TYPE

Cite this: DOI: 10.1039/xxxxxxxxxx

Exploring Electron Pair Behaviour in Chemical Bonds using the Extracule Density†

Adam J. Proud, Dalton E.C.K. Mackenzie, and Jason K. Pearson*

Received Date
Accepted Date

DOI: 10.1039/xxxxxxxxxx

www.rsc.org/journalname

We explore explicit electron pair behaviour within the chemical bond (and lone pairs) by calculating the probability distribution for the center-of-mass (extracule) of an electron pair described by single localized orbitals. Using Edmiston-Ruedenberg localized orbitals in a series of 61 chemical systems, we demonstrate the utility of the extracule density as an interpretive tool in chemistry. By accessing localized regions of chemical space we simplify the interpretation of the extracule density and afford a quantum mechanical interpretation of "chemically intuitive" features of electronic structure. Specifically, we describe the localized effects on chemical bonds due to changes in electronegativities of bonded neighbours, bond strain, and non-covalent interactions. We show that the extracule density offers unique insight into electronic structure and allows one to readily quantify the effects of changing the chemical environment.

1 Introduction

The molecular wavefunction contains a wealth of information; however, the Schrödinger equation[1] consists solely of one and two-electron operators. Thus, much of the information contained in the wavefunction is superfluous. Hohenberg and Kohn[2] demonstrated that the energy of a chemical system can be obtained, using only the electron density, $\rho(\mathbf{r})$,

$$\rho(\mathbf{r}) = \int |\Psi(\mathbf{r_1}, \mathbf{r_2}, \ldots, \mathbf{r_N})|^2 \mathrm{d}\mathbf{r_2} \ldots \mathrm{d}\mathbf{r_N} \quad (1)$$

where $\mathbf{r_i}$ denotes the position vector of electron i. While one may be able to determine the energy from $\rho(\mathbf{r})$, extracting useful information regarding electron-electron interactions is inherently nonintuitive. More useful is the pair density, $\rho(\mathbf{r_1}, \mathbf{r_2})$, which we define as

$$\rho(\mathbf{r_1}, \mathbf{r_2}) = \int |\Psi(\mathbf{r_1}, \mathbf{r_2}, \ldots, \mathbf{r_N})|^2 \mathrm{d}\mathbf{r_3} \ldots \mathrm{d}\mathbf{r_N} \quad (2)$$

As this function contains information regarding the simultaneous positions of two electrons, a description of interelectronic interactions is readily accessible. The main difficulty rests in the interpretation of the pair density. Visual representation is a powerful analytical tool; however, being a function of 6 coordinates, graphical representation of the pair density is not feasible and manipulations to $\rho(\mathbf{r_1}, \mathbf{r_2})$ must be carried out to extract useful information. One such manipulation results in the intracule density, $P(u)$,[3] which is defined as:

$$P(u) = \int \rho(\mathbf{r_1}, \mathbf{r_2}) \delta(u - |\mathbf{r_1} - \mathbf{r_2}|) \mathrm{d}\mathbf{r_1} \mathrm{d}\mathbf{r_2} \mathrm{d}\Omega_u \quad (3)$$

where u is the interelectronic distance, $\delta(x)$ is the one-dimensional Dirac delta function and Ω_u denotes the integration over the angular components of the $\mathbf{u}$ vector. The utility of this density is rather obvious as electron repulsion energies are directly related to the interelectronic distance, u. The main deficiency in $P(u)$ is the absence of any *absolute* position information. It provides no insight as to where in the molecular system the electrons are most likely to reside.[4] One way we can extract such information is through the extracule density, $E(\mathbf{R})$, which describes the probability of finding the centre-of-mass of an electron pair at the position described by the vector $\mathbf{R}$ (we shall simply refer to the centre-of-mass of an electron pair as the centre-of-mass. This is not to be confused with the centre-of-mass of the molecule).[5,6] This density can be obtained from the pair density by:

$$E(\mathbf{R}) = \int \rho(\mathbf{r_1}, \mathbf{r_2}) \delta\left(\mathbf{R} - \tfrac{\mathbf{r_1}+\mathbf{r_2}}{2}\right) \mathrm{d}\mathbf{r_1} \mathrm{d}\mathbf{r_2} \quad (4)$$

The extracule density was first described by Coleman in the late 1960s[7]; however, it wasn't until the early 1980s when the first calculations of $E(\mathbf{R})$ were carried out.[5] Since the seminal paper by Thakkar and Moore, studies regarding the topology of $E(\mathbf{R})$ have largely been focused on the spherically averaged extracule density, $E(R)$, defined as

$$E(R) = \int E(\mathbf{R}) \, \mathrm{d}\Omega_R \quad (5)$$

University of Prince Edward Island, Department of Chemistry, 550 University Avenue, Charlottetown, PE, Canada, C1A 4P3, Tel: 1-902-566-0394; E-mail: jpearson@upei.ca

† Electronic Supplementary Information (ESI) available: [ESI contains information regarding extracules of second row hydrides]. See DOI: 10.1039/b000000x/

or a single dimension of $E(\mathbf{R})$.[8–17] While this scalar form may be useful for linear systems, the complexity of the interpretation for large systems is readily apparent since the number of pairs of electrons grows as $N(N-1)/2$ where N is the number of electrons. Knowing only the distance of the centre-of-mass from a specified origin is not generally very informative in a three-dimensional molecule. For this reason, we have focused on the more topologically rich, $E(\mathbf{R})$ for the purposes of this study.

While $E(\mathbf{R})$ does offer more clarity into the distribution of the centre-of-mass, difficulty still arises in its interpretation when one considers arbitrarily large 3D structures. Thus, it is rather useful to consider a single electron pair as opposed to all electron pairs in a chemical system. For this reason, we have recently developed the Localized Pair Model (LPM) for localized electronic structure analysis.[18,19] The concept is based on the use of localized molecular orbitals (LMOs) which are far more chemically intuitive than the traditional or canonical molecular orbitals (CMOs) which are often delocalized over the entire molecule. LMOs represent important chemical concepts such as chemical bonds and lone pairs. The other major benefit is that by analyzing a single molecular orbital, there is only a single pair of electrons and thus, the extracule density describes the centre-of-mass of that specific electron pair within that chemical bond or lone pair.

The idea of LMOs was first conceptualized by Lennard-Jones and Pople in the 1950s,[20,21] but it wasn't until the 1960s that algorithms for their calculation were developed. As LMOs are essentially linear combinations of CMOs, one can imagine that there are numerous ways in which they can be constructed.[22–25] Lennard-Jones and Pople originally theorized that one could obtain a set of LMOs by minimizing the following expression which describes the interorbital repulsions[20,21]:

$$4\sum_{i}\sum_{j>i}\int\int|\psi_i(\mathbf{r_1})|^2\frac{1}{r_{12}}|\psi_j(\mathbf{r_2})|^2\mathrm{d}\mathbf{r_1}\mathrm{d}\mathbf{r_2} \tag{6}$$

where $\psi_i(\mathbf{r_k})$ is the i^{th} molecular orbital. The Edmiston-Ruedenberg (ER) localization method[23] is based on this property of minimizing interorbital repulsions. Developed in the 1960s, this method remains as one of the most robust today, although it requires significant computational resources relative to alternative localization schemes. Other methods, such as Foster-Boys (FB) localization[22] focuses instead on maximizing the distance between the centroids of charge of each LMO and is significantly faster than the ER algorithm. However, in a previous study,[18] we noted that while the determination of Edmiston-Ruedenberg LMOs may be more computationally intensive, it does generate "chemically intuitive" orbitals and rarely encounters problems in the computation of the LMOs. The LPM can be applied to any type of orbital such as natural bond orbitals (NBOs),[26–30] intrinsic bond orbitals (IBOs),[31,32] absolutely localized molecular orbitals (ALMOs),[33–38] as well as canonical molecular orbitals. However, herein we focus on localized features of electronic structure and all data presented was determined using ER LMOs.

2 Computational Methods

If the pair density is determined from a RHF wavefunction, equation (4) may be expressed as

$$E(\mathbf{R}) = \sum_{\mu\nu\lambda\sigma}^{K}\Gamma^{\mathrm{HF}}_{\mu\nu\lambda\sigma}(\mu\nu\lambda\sigma)_E \tag{7}$$

where $\Gamma^{\mathrm{HF}}_{\mu\nu\lambda\sigma}$ is the HF two-particle density matrix and $(\mu\nu\lambda\sigma)_E$ are the extracule integrals evaluated over the basis functions μ, ν, λ, and σ. These integrals are described by

$$(\mu\nu\lambda\sigma)_E = \int\phi^*_\mu(\mathbf{r})\,\phi_\nu(\mathbf{r})\,\phi^*_\lambda(2\mathbf{R}-\mathbf{r})\,\phi_\sigma(2\mathbf{R}-\mathbf{r})\,\mathrm{d}\mathbf{r} \tag{8}$$

Herein, ϕ_i denotes basis function i. Thakkar and Moore developed a series of formulae for the determination of the extracule integrals, which are summarized below.[5] These equations were utilized to calculate the necessary integrals for the evaluation of $E(\mathbf{R})$ for a specific LMO. For a basis set consisting of Gaussian-type orbitals, the basic integral over four s-type Gaussians is given by

$$(ssss)_E = \left(\frac{4\pi}{\zeta+\eta}\right)^{3/2}\exp\left[-\frac{\zeta\eta(2\mathbf{R}-\mathbf{P}-\mathbf{Q})^2}{\zeta+\eta}\right] \times \exp\left[-\frac{\alpha\beta(\mathbf{A}-\mathbf{B})^2}{\zeta}-\frac{\gamma\delta(\mathbf{C}-\mathbf{D})^2}{\eta}\right] \tag{9}$$

where $\mathbf{A}$, $\mathbf{B}$, $\mathbf{C}$, and $\mathbf{D}$ define the centres on which the gaussian primitives, with exponents α, β, γ, and δ, respectively, are centred. These exponents comprise $\zeta=\alpha+\beta$ and $\eta=\gamma+\delta$. The variables $\mathbf{P}$ and $\mathbf{Q}$ are defined as follows:

$$\mathbf{P} = \frac{\alpha\mathbf{A}+\beta\mathbf{B}}{\zeta} \tag{10}$$

$$\mathbf{Q} = \frac{\gamma\mathbf{C}+\delta\mathbf{D}}{\eta}$$

For integrals containing orbitals of higher angular momenta, these new integrals can be determined by multiplying the basic integral by the angular factors, T_x, T_y, and T_z:

$$(\mu\nu\lambda\sigma)_E = (ssss)_E T_x T_y T_z \tag{11}$$

To define the angular factors (we will define the variables with respect to the angular factor in the x-axis, T_x, but these can easily be adapted to determine the y and z directional angular factors by using the respective components for those directions), we must first introduce the following three variables:

$$g_k = \left(-\frac{\zeta+\eta}{4\zeta\eta}\right)^k \times \frac{1}{k!} \tag{12}$$

$$h_k = (P_x+Q_x-2R_x)^k \times \frac{1}{k!} \tag{13}$$

$$s_k = \frac{1}{g_k}\sum_{j=0}^{k/2} g_j h_{k-2j} \tag{14}$$

where $0\le k\le l_\mu+l_\nu+l_\lambda+l_\sigma$ in which l_i denotes the angular momentum of gaussian primitive i, in the x-axis. Using these newly

defined variables, T_x can be computed using

$$T_x = \sum_{i=0}^{l_\mu+l_\nu} \Lambda_i(l_\mu, l_\nu, P_x - A_x, P_x - B_x, \zeta) \quad (15)$$

$$\times \sum_{j=0}^{l_\lambda+l_\sigma} s_{i+j}\Lambda_j(l_\lambda, l_\sigma, Q_x - C_x, Q_x - D_x, \eta)$$

where

$$\Lambda_j(l_1, l_2, a, b, c) = \sum_{k=0}^{(l_1+l_2-j)/2} f_{2k+j}(l_1, l_2, a, b)\frac{(2k+j)!}{(4c)^{k+j}k!\,j!} \quad (16)$$

Herein, f_j can be defined as the polynomial coefficients obtained from:

$$\sum_{j=0}^{l_1+l_2} f_j(l_1, l_2, a, b)x^j = (x+a)^{l_1}(x+b)^{l_2} \quad (17)$$

As the three angular factors are equal to unity for a set of four *s*-type Gaussians, equation (11) is a general formula that can be used in the evaluation of all extracule integrals.

To calculate the extracule densities, a Mura-Knowles grid[39] was utilized to determine the value of $E(R_x, R_y, R_z)$ at each grid point which was succeeded by interpolation to yield the required functions. This grid was adapted for the inclusion of negative values by incorporating grid points in both the positive and negative directions to ensure that all relevant spatial regions of the chemical system were adequately described. In order to obtain grids that were sufficiently dense to converge the resulting extracules, 201 points (100 points in each of the positive and negative directions in addition to the origin) were used in two of the three dimensions. These calculations would scale as $(K^4) \times (n_p^d)$ where d indicates the number of dimensions sampled and n_p defines the number of grid points in each dimension. As one dimension would necessarily be averaged through integration for purposes of visual representation, the benefit of sampling all three dimensions was deemed to be insufficient to warrant the computational cost. Thus, for the extracule density analysis of all molecular systems, the atoms important to the analysis were positioned in the *yz*-plane over which the grid was constructed.

All calculations were performed at the RHF/u6-311G(d,p) level of theory where u indicates that the basis set was completely uncontracted. HF calculations are adequate for these systems as the goal is to demonstrate the utility of the extracule density in the LPM as an interpretive tool in chemistry; however, should an alternative approach be desired, Kohn-Sham orbitals[40] could be employed in an identical fashion. All geometry optimizations and LMO determinations were performed using the GAMESS software package.[41] Vibrational frequency analyses were conducted to ensure that the geometry represented an energy minimum. After computing the extracule densities using the Mura-Knowles grid, the data was analyzed using the Mathematica 8 software package.[42] Atomic units are used throughout.

3 Results and Discussion

3.1 Covalent Bonding

We begin with the hydrides of first row elements, i.e. LiH to HF. Two sets of analyses were carried out for this set. In Case 1, full geometry optimizations were performed on the molecules and these optimized structures were used in the analysis. For Case 2, the average bond length for the X-H (X = Li – F) bonds from Case 1 were determined and the optimized structures were then modified to include this average bond length *solely* for the bond to be analyzed. Thus, for NH_3, two of the N-H bonds would remain at the length determined through the geometry optimization, and only the one bond that was to be analyzed was adjusted to the average X-H bond length determined from the set of hydrides. Case 2 allows for a convenient comparison of the bond extracule densities as the nuclei involved in the hydride-bond LMO are at the same positions in Cartesian space.

Figure 1(a) depicts the extracule density for the C-H bond in methane. One might expect that the maximum in the density would occur closer to the carbon atom considering its slightly more electronegative nature; however, one must consider the structure of the molecular orbital. As observed from the overlaid orbital representation, the C-H bond LMO largely resembles depictions of sp^3 orbitals common in freshman and organic chemistry textbooks.[43,44] Much of the density of the orbital extends out from the carbon atom beyond the hydrogen atom. This results in the electrons in the orbital being shifted more towards the hydrogen atom than one might initially expect.

What is more enlightening is observing the shift in the maximum as one changes the heavy atom from the highly electropositive Li atom to the highly electronegative F atom. These results are tabulated in Table 1. For all systems, the bond midpoint is positioned at (0,0,0) in Cartesian space. For the purposes of this discussion, the only coordinate listed is that which occurs along the bond axis, R_z. The R_y coordinate was close to 0 for all cases, but the small deviations can be explained by the asymmetric inductive effects caused by the other atoms within the molecules. As the heavy atom in the molecule is modified from Li to F, the maximum in the extracule density shifts toward the heavy atom. What may be less obvious is the extent to which the centre-of-mass is shifting. This becomes far more evident as we examine $R_z^{\max}$ for Case 2. For all molecules in Case 2, the two nuclei are positioned at $R_z = \pm 1.08646$ with the heavy atom residing in the positive direction. For the case of the Li atom, the maximum in $E(0, R_y, R_z)$ occurs at $R_z = -1.028$, which is very close to the hydrogen nucleus. As we change our heavy atom from N to O, the centre-of-mass maximum shifts beyond the bond midpoint towards the heavy atom. In the most extreme case, HF, the maximum in the extracule density is found nearly halfway between the bond midpoint and the heavy F atom at $R_z = 0.500$. These same trends of the centre-of-mass shifting towards the electronegative atom are observed in the average R_z value, $\langle R_z \rangle$, which is given by

$$\langle R_z \rangle = \frac{1}{\langle R_{yz}^0 \rangle}\int_{-\infty}^{\infty}\int_{-\infty}^{\infty} R_z \times E(0, R_y, R_z)\mathrm{d}R_y\mathrm{d}R_z \quad (18)$$

where $\langle R_{yz}^0 \rangle$ is the zeroth moment in the bond plane (defined be-

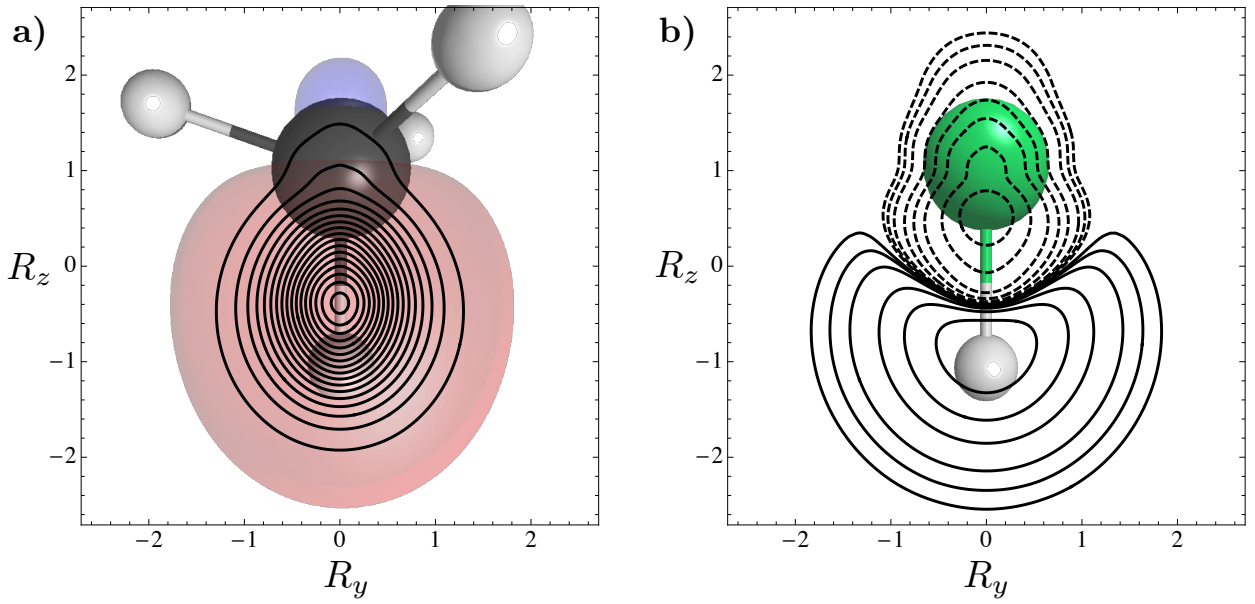

Fig. 1 a) Depiction of $E(0,R_y,R_z)$ for the C-H bond in CH_4 with an overlay of the LMO for the bond and b) $\Delta E^{H_3C,F}(0,R_y,R_z)$ for the X-H bond LMO. Contour values were chosen as $m\times10^{-n}$, where $m=2,4$ and 8 and $n=3,2,$ and 1 (the dashed lines signify negative contours).

low in equation 19). As we consider only a slice of $E(\mathbf{R})$, $\langle R_z\rangle$ must be scaled by this value to obtain an accurate value for the average R_z. While the shift in the centre-of-mass towards the heavy atom as the electronegativity of that heavy atom increases is not surprising, it does demonstrate that the localized extracule density displays the effects one would expect based on chemical intuition. Less obvious is the trend observed in $\langle R^0_{yz}\rangle$, which is defined as

$$\langle R^0_{yz}\rangle = \int_{-\infty}^{\infty}\int_{-\infty}^{\infty} E(0,R_y,R_z)\mathrm{d}R_y\mathrm{d}R_z \qquad (19)$$

Because slices of the extracule density were chosen as opposed to averaging over one coordinate, the zeroth moment is not normalized to $\frac{N(N-1)}{2}$, as it otherwise would be. Instead, we obtain information regarding the amount of extricable density that resides within the given slice. Specifically, $\langle R^0_{yz}\rangle$, is the value of $E(R_x)$ where $R_x=0$ and the remaining Cartesian coordinates have been averaged through integration. We note that $\langle R^0_{yz}\rangle$ is not bounded by 1 (as can be confirmed in Table 1), as a probability normally would be because it is not evaluated over a range in the x coordinate. One clear trend emerges as we change the identity of the heavy atom. The introduction of the more electronegative heavy atoms causes a contraction of the centre-of-mass to the bonding plane. While $\langle R^0_{yz}\rangle=0.512$ in the case of LiH, this value nearly doubles to 0.982 upon replacing Li with the highly electronegative F. This observation is in strong agreement with the tendency of the electron-electron counterbalance density[45–49] for the helium isoelectronic series (from He to Ne^{8+}) to increase as the nuclear charge, and thus electronegativity, is increased.[47] Equivalent analyses were performed on the second row hydrides which are not shown as all of the trends were identical to those shown here.

The major benefit offered by the equidistant bond lengths analyzed in Case 2 is that one can accurately assess the extracule

Table 1 Moments of $E(0,R_y,R_z)$ for the X-H bond LMO in first row hydrides.

	Case 1			Case 2		
System	$\langle R^0_{yz}\rangle$	$\langle R_z\rangle$	R_z^{max}	$\langle R^0_{yz}\rangle$	$\langle R_z\rangle$	R_z^{max}
LiH	0.473	-1.280	-1.453	0.512	-1.022	-1.028
BeH_2	0.557	-0.848	-0.996	0.595	-0.764	-0.836
BH_3	0.664	-0.579	-0.600	0.674	-0.570	-0.592
CH_4	0.743	-0.353	-0.383	0.728	-0.356	-0.385
NH_3	0.832	-0.181	-0.219	0.791	-0.157	-0.221
OH_2	0.932	-0.046	0.055	0.872	0.024	0.294
FH	1.047	0.091	0.272	0.982	0.218	0.500

deformation density, $\Delta E^{X_1,X_2}(0,R_y,R_z)$, which is given by

$$\Delta E^{X_1,X_2}(0,R_y,R_z) = E^{X_1\text{-}H}(0,R_y,R_z) - E^{X_2\text{-}H}(0,R_y,R_z) \qquad (20)$$

where X_i-H represents the LMO describing the hydride bond in the system of interest. With the positions of the two nuclei involved in the bond LMO fixed for all systems, all changes in $\Delta E^{X_1,X_2}(0,R_y,R_z)$ can be attributed to the changing chemical environment. An example is shown in Figure 1(b) where $X_1=CH_3$ and $X_2=F$. As expected, the negative contours are present near the heavy atom indicating the greater presence of the electron pair centre-of-mass near the heavy atom in the HF system compared to CH_4. Likewise, positive values of $\Delta E^{CH_3,F}(0,R_y,R_z)$ are present near the hydrogen atom as the electron density and consequently the centre-of-mass of the electron pair are drawn towards the fluorine atom in HF.

Following the analysis of the hydrides, the localized pair model was used to analyze compounds consisting of the -CH_3, -NH_2, -OH, and -F fragments from the first row and the -SiH_3, -PH_2, -SH, and -Cl fragments from the second row. Forming covalent compounds from any two of these moieties results in 10 compounds

from each of the first and second row and 16 compounds from the combination of building blocks from separate rows. Thus 36 compounds were constructed and analyzed in terms of the extracule densities for the bond between the two heavy atoms as well as the X-H bond for both heavy atoms in each fragment. As for the first and second row hydrides, the bond midpoint is positioned at (0,0,0) in Cartesian space with the heavy atom (or in the case of the X_1-X_2 bond, the X_1 atom) positioned in the positive R_z direction.

The results for these systems are listed in Table 2. For the LMO describing the bond between the two heavy atoms, X_1 and X_2, the same trends described in the previous section are evident for *most* species. We observe a substantial migration of the centre-of-mass into the bond plane as we increase the electronegativity of either heavy atom. Furthermore, the more obvious shifting of the centre-of-mass towards X_2 is evident as the electronegativity of X_2 increases. When considering a substitution from first row to second row heavy atoms, a significant decrease in $\langle R^0_{yz}\rangle$ is observed universally. This is indicative of a lower likelihood of observing R in the yz bond plane. Considering the significant size disparity between these rows, one might expect such a trend as the electrons in second row atoms would accommodate a larger volume outside of the selected bond plane leading to this observed decrease in $\langle R^0_{yz}\rangle$.

Once we shift to the X_i-H bond LMO, X_j is no longer directly part of the LMO of interest, but is instead separated by one bond. As LMOs are, by definition, *localized*, the changes in the extracule density are expected to be minimal when the two atoms comprising the bond LMO remain the same. In these cases, the trends appear to vanish; however, there are a number of competing factors at play. First, we have the aforementioned enhancement of the inductive effect caused by the increasing electronegativity of X_2 drawing the electron density, and thus the centre-of-mass towards X_2. Other related effects include the effect that X_2 has on the shape of the localized orbital in question as well as its effect on the bond lengths between X_1-H and X_1-X_2. Considering all of these factors, it is not surprising that there is no obvious trend in $\langle R^1_z\rangle$ and $R^{\max}_z$ for the X-H bonds in these systems. However, the increase in $\langle R^0_{yz}\rangle$ is still evident as the electronegativity of the non-participating heavy atom is increased.

To further explore the effects of electronegativity on the extracule density, we analyzed methane with varying levels of halogenation. Both the C-X and CH bonds of $CH_{4-n}F_n$ and $CH_{4-n}Cl_n$ (where $n = 0-4$) were explored. Figure 2 depicts the position of the maximum in the case of the C-H bond extracules for the $CH_{4-n}F_n$ systems. The introduction of the fluorine atoms cause an obvious shift in $\mathbf{R}_{\max}$ within the C-H bond plane and *away* from the internuclear axis. The quantitative measures for these halogenated systems as well as those containing Cl are summarized in Table 3 and indicate that the extracular LPM has the capabilities to discern small but significant anisotropies in the topology of electron-electron interactions within the chemical bond.

With the overlaid structures depicting the positions of halogenation in Figure 2, the positioning is explained based on the inductive effects of the newly introduced electronegative atom. Upon the addition of the three halogens for the analysis of the C-H bond, the maximum returns to the bond axis due to the symmetry around the tetrahedral carbon, but it is significantly shifted towards the three halogen atoms. These same trends can be observed for the C-H bonds in the chlorinated systems as well as the C-X bonds in both sets of halogenated molecules.

Table 3 Properties of $E(0,R_y,R_z)$ for halogenated derivatives of methane.

	C-H Bond		C-X Bond	
System	$\langle R^0_{yz}\rangle$	(R_y,R_z) of Max	$\langle R^0_{yz}\rangle$	(R_y,R_z) of Max
CH_4	0.745	(0.000, 0.383)	- - -	- - -
CH_3F	0.760	(0.013, 0.365)	1.037	(0.000, 0.686)
CH_2F_2	0.782	(0.005, 0.346)	1.053	(0.009, 0.651)
CHF_3	0.797	(0.000, 0.324)	1.065	(0.004, 0.618)
CF_4	- - -	- - -	1.070	(0.000, 0.589)
CH_4	0.745	(0.000, 0.383)	- - -	- - -
CH_3Cl	0.760	(0.015, 0.357)	0.722	(0.000, 0.036)
CH_2Cl_2	0.772	(0.007, 0.337)	0.732	(0.016, -0.116)
$CHCl_3$	0.783	(0.000, 0.320)	0.736	(0.007, -0.127)
CCl_4	- - -	- - -	0.743	(0.000, -0.136)

3.2 Bond Strain

An ideal tetrahedral carbon has sp^3 hybridization with bond angles of 109.5°. However, for some cycloalkanes, this conformation is simply not possible. For instance, cyclopropane, a well documented example,[50–52] contains significant amounts of strain due to its triangular conformation deviating significantly from the optimal configuration around a *tetrahedral* carbon. This strain causes the formation of "bent bonds" or "banana bonds". This bending is clearly observed in the extracule density of not only cyclopropane but also to some extent, in cyclobutane (Figure 3). The bending in $E(\mathbf{R})$ effectively vanishes in the densities calculated for cyclopentane and cyclohexane. A quantitative analysis can be performed by determining the position of the maximum in $E(\mathbf{R})$ outside of the bond axis, i.e. R_y. This measure is tabulated in Table 4. The maximum for cyclopropane is observed at $R^{\max}_y = 0.349$ for cyclopropane but migrates towards the bond axis as the ring strain decreases and essentially resides in the bond axis for the "strainless" cyclohexane.

To accommodate the smaller angles involving the C-C bonds in the smaller cycloalkanes, the orbitals take on significantly more p-character than a typical C-C bond between *tetrahedral* carbons. In the case of cyclopropane, the carbon atoms participating in the C-C bonds are considered to be sp^5 hybridized with respect to that orbital.[50] As the size of the ring in the cycloalkane increases, the strain is relieved and the amount of p-character in the bonds decrease. As p-orbitals are less electronegative than s-orbitals, progressing from cyclopropane to cyclohexane, we would expect the electronegativity of the carbon involved in the C-C bond to increase, leading to an increase in the proportion of $E(\mathbf{R})$ present in the bond plane. This prediction is confirmed by the values of $\langle R^0_{yz}\rangle$ provided in Table 4.

Table 2 Analysis of the X_1-X_2 and X_i-H bond LMOs in small first and second row compounds.

	X_1-X_2 Bond			X_1-H Bond			X_2-H Bond		
System	$\langle R^0_{yz}\rangle$	$\langle R_z\rangle$	R_z^{max}	$\langle R^0_{yz}\rangle$	$\langle R_z\rangle$	R_z^{max}	$\langle R^0_{yz}\rangle$	$\langle R_z\rangle$	R_z^{max}
CH_3CH_3	0.752	0.000	0.000	0.749	-0.362	-0.386	0.749	-0.362	-0.386
CH_3NH_2	0.828	-0.183	-0.111	0.750	-0.384	-0.388	0.841	-0.189	-0.220
CH_3OH	0.928	-0.348	-0.493	0.759	-0.357	-0.370	0.950	-0.047	0.025
CH_3F	1.037	-0.477	-0.686	0.760	-0.365	-0.365	- - -	- - -	- - -
CH_3SiH_3	0.636	0.488	0.487	0.742	-0.335	-0.382	0.609	-0.865	-0.968
CH_3PH_2	0.661	0.298	0.284	0.749	-0.340	-0.374	0.651	-0.672	-0.771
CH_3SH	0.686	0.063	0.173	0.754	-0.331	-0.369	0.692	-0.465	-0.592
CH_3Cl	0.722	-0.154	-0.036	0.761	-0.333	-0.357	- - -	- - -	- - -
NH_2NH_2	0.885	0.004	0.000	0.843	-0.199	-0.217	0.843	-0.199	-0.217
NH_2OH	0.958	-0.174	-0.064	0.852	-0.190	-0.205	0.956	-0.057	0.030
NH_2F	1.054	-0.358	-0.630	0.858	-0.184	-0.195	- - -	- - -	- - -
NH_2SiH_3[a]	0.743	0.736	0.848	0.830	-0.209	-0.204	0.612	-0.888	-0.974
NH_2PH_2[a]	0.750	0.532	0.655	0.834	-0.181	-0.200	0.654	-0.702	-0.778
NH_2SH	0.764	0.333	0.323	0.842	-0.182	-0.199	0.695	-0.469	-0.583
NH_2Cl	0.775	0.102	0.188	0.854	-0.183	-0.194	- - -	- - -	- - -
OHOH	1.011	0.008	0.000	0.963	-0.044	0.060	0.963	-0.044	0.060
OHF	1.093	-0.197	-0.044	0.970	-0.036	0.080	- - -	- - -	- - -
$OHSiH_3$	0.872	0.791	0.893	0.939	-0.020	0.047	0.613	-0.881	-0.962
$OHPH_2$	0.872	0.678	0.843	0.946	-0.026	0.048	0.656	-0.700	-0.771
OHSH	0.863	0.532	0.798	0.954	-0.033	0.053	0.697	-0.473	-0.582
OHCl	0.857	0.343	0.283	0.960	-0.030	0.067	- - -	- - -	- - -
FF	1.152	0.000	0.000	- - -	- - -	- - -	- - -	- - -	- - -
$FSiH_3$	1.008	0.857	0.953	- - -	- - -	- - -	0.615	-0.860	-0.940
FPH_2	0.998	0.788	0.942	- - -	- - -	- - -	0.659	-0.678	-0.751
FSH	0.978	0.693	0.939	- - -	- - -	- - -	0.700	-0.458	-0.569
FCl	0.965	0.556	0.919	- - -	- - -	- - -	- - -	- - -	- - -
SiH_3SiH_3	0.502	0.000	0.000	0.608	-0.837	-0.962	0.608	-0.837	-0.962
SiH_3PH_2	0.544	-0.251	-0.033	0.611	-0.838	-0.952	0.647	-0.644	-0.765
SiH_3SH	0.594	-0.489	-0.458	0.613	-0.838	-0.943	0.687	-0.443	-0.589
SiH_3Cl	0.652	-0.673	-0.652	0.615	-0.829	-0.930	- - -	- - -	- - -
PH_2PH_2	0.574	0.002	0.000	0.652	-0.649	-0.757	0.652	-0.649	-0.757
PH_2SH	0.612	-0.274	-0.031	0.655	-0.652	-0.750	0.690	-0.447	-0.582
PH_2Cl	0.662	-0.519	-0.541	0.658	-0.644	-0.739	- - -	- - -	- - -
SHSH	0.642	-0.011	0.000	0.694	-0.448	-0.576	0.695	-0.313	-0.576
SHCl	0.678	0.270	0.024	0.698	-0.438	-0.566	- - -	- - -	- - -
ClCl	0.710	0.000	0.000	- - -	- - -	- - -	- - -	- - -	- - -

[a] The LMO for this X_1-X_2 bond showed significant distortion relative to the others. The maximum in $E(0,R_y,R_z)$ deviated from the bond axis, R_z, by > 0.050 a.u.

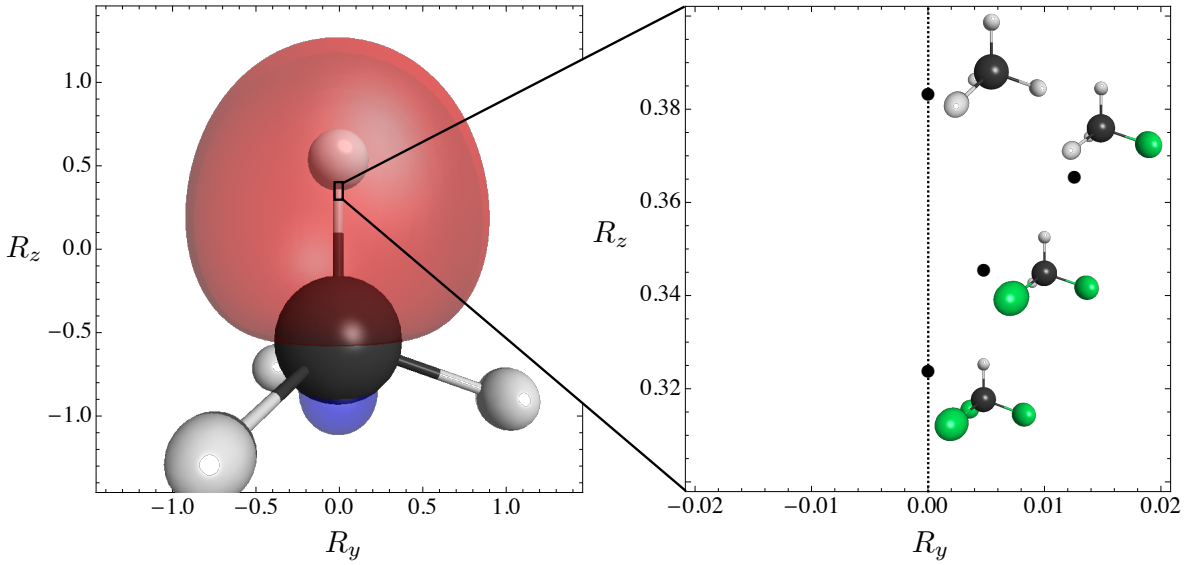

Fig. 2 Pictorial representation of CH_4 to demonstrate the positions of each atom within the molecule combined with an inset of the positions of the maxima of $E(0,R_y,R_z)$ for the C-H bond in methane and its fluorinated derivatives, CH_nF_{3-n}, where $n = 1-3$ (the dashed line signifies the bond axis).

Table 4 Properties of $E(0,R_y,R_z)$ for the C-C bonds in cycloalkanes.

System	$\langle R^0_{yz}\rangle$	$R^{\max}_y$
Cyclopropane (C_3H_6)	0.750	0.349
Cyclobutane (C_4H_8)	0.751	0.099
Cyclopentane (C_5H_{10})	0.755	0.017
Cyclohexane (C_6H_{12})	0.757	-0.004

3.3 Non-Covalent Interactions

While LMOs are largely local in nature, as demonstrated above, they are influenced in characteristic ways by their neighbouring chemical environments. This suggests that the LPM has utility in analyzing non-covalent interactions. For example, hydrogen bonding may be interpreted as the interaction between an electron rich lone pair of a donor species with an electron deficient acceptor species. The extent and/or character of the interaction may then be probed by observing changes in the distributions of localized electron pairs on either the donor or acceptor species (or both). Here, we have modelled the hydrogen bonding interaction between HF and $MeNH_2$ through the σ_{HF} bond LMO of HF and the n_N lone pair LMO on the $MeNH_2$ nitrogen. Accurate geometries for the hydrogen bonding complex were obtained from the S66x8 data set.[53] Extracule calculations were performed on the H-F bond in the absence of $MeNH_2$ (and vice versa) and with varying separations between the HF and $MeNH_2$ molecules. The b_0 separation indicates that the distance between the hydrogen bond donor and acceptor is that which is obtained from the geometry optimization carried out at the MP2/cc-pVTZ level. Systems denoted by $x \times b_0$ indicate that the distance between the two species, d, is scaled proportionally to x. Thus, the HF-MeOH complex where $d = 2.0b_0$ contains an H-bond distance that is twice the value obtained in the geometry optimization. All other geometrical parameters remain the same. For the HF bond, the bond midpoint was positioned at the origin in Cartesian space, while for the lone pair, the nitrogen atom in methylamine was positioned at (0,0,0.945) while the H in hydrogen fluoride was positioned along the R_z axis at positions relative to the separation of the two species. The positioning of the nitrogen atom was chosen to allow for adequate sampling of $E(0,R_y,R_z)$ using the previously described grid points.

Our goal in analyzing the extracule density of these LMOs was to observe the effect on the extracule density as the hydrogen bond formed and how those effects varied as the distance between the two species grew. Thus we analyzed the extracule deformation density of orbital ϕ, $\Delta E^{\phi}_d(\mathbf{R})$, which we define in this case as

$$\Delta E^{\phi}_d(\mathbf{R}) = E^{\phi,\text{complex}}_d(\mathbf{R}) - E^{\phi,\text{molecule}}(\mathbf{R}) \qquad (21)$$

which parametrically depends on d, the distance between the species in the molecular complex.

These results are depicted in Figure 4. For the HF bond, the figure clearly shows an increase in $E(R)$ near the F atom as the hydrogen bond forms. This effect diminishes significantly as the distance separating the species varies from $d = 0.9b_0$ to $d = 2.0b_0$ ($0.9b_0$ not shown). This change can be concisely rationalized by the migration of electrons during the formation of a hydrogen bond. In this case, the H atom in H-F would interact with the electron density of the donor lone pair in $MeNH_2$. Interacting with the nitrogen, allows the electrons within the H-F bond to migrate towards the F atom resulting in the increase in the likelihood of the centre-of-mass of that electron pair to be close to fluorine. Conversely, when considering the lone pair in $MeNH_2$, we observe a decrease in the extracule deformation density near the nitrogen atom and an increase in the internuclear region between N and the HF molecule. Unlike the H-F bond where the hydrogen-fluorine interaction was weakening, here the nitrogen-hydrogen interaction is becoming stronger. Thus, the electrons are migrating toward the hydrogen and consequently shifting the

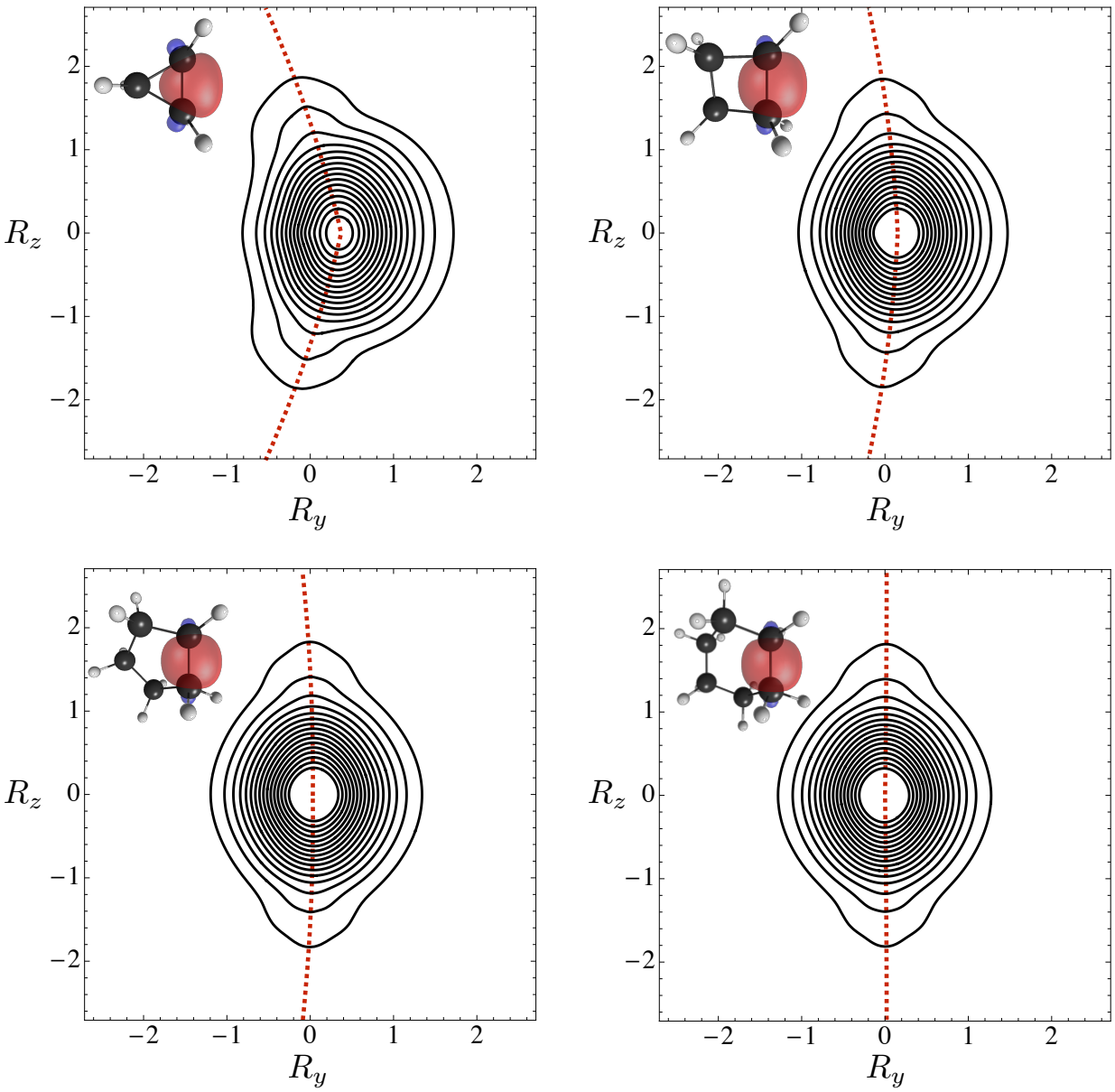

Fig. 3 Depiction of $E(\mathbf{R})$ for representative C-C bonds in the cyclic systems ranging from cyclopropane to cyclohexane. Models of the appropriate molecule are inlayed in the top left hand corner of each graph to provide the reader with insight as to the spatial orientation of each molecule. The dashed line traces the curve of slowest descent in $E(R_y, R_z)$ to illustrate the deviation from the bond axis. Contour values were chosen as $0.02 \times n$ where $n = 1 - 16$.

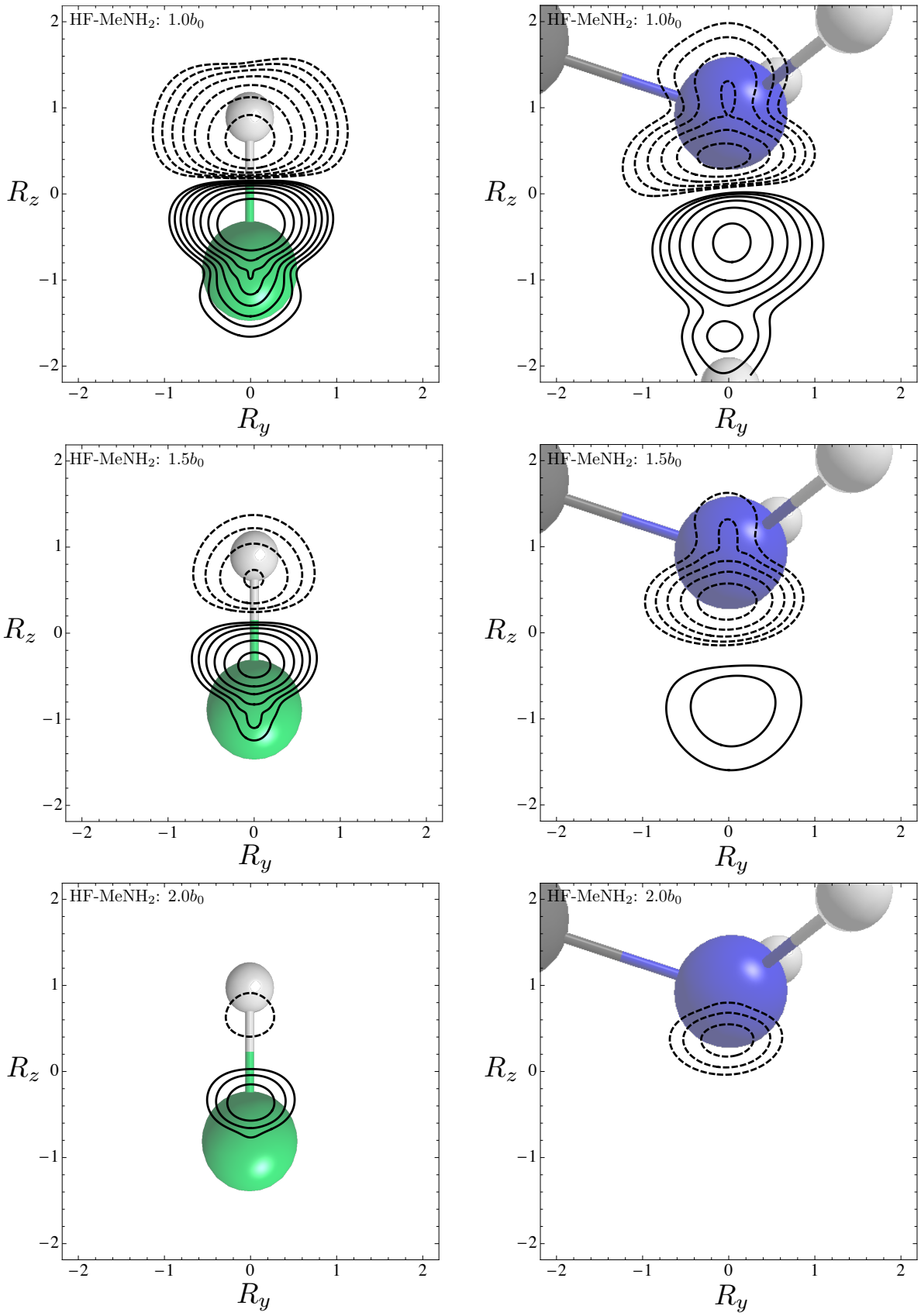

Fig. 4 Depiction of $\Delta E_d^{\phi}(\mathbf{R})$ for the σ_{HF} bond LMO in H-F (left) and the n_N lone pair LMO in $MeNH_2$ (right) for the HF-$MeNH_2$ hydrogen bonded complex at various distances of separation, $x \times b_0$, between the donor and acceptor. Contours were chosen as $\pm 0.003 \times 1.5^n$ where $n = 1 - 8$. Negative contours are denoted by dashed lines.

Table 5 Properties of $E_d^{\phi,\text{HF-MeNH}_2}(0,R_y,R_z)$ and $\Delta E_d^{\phi}(0,R_y,R_z)$ for the HF bond (σ_{HF}) and the $MeNH_2$ lone pair (n_N) LMOs.

	$E_d^{\phi,\text{HF-MeNH}_2}$		ΔE_d^{ϕ}	
Molecule, ϕ	$\langle R_{yz}^0 \rangle$	R_z^{max}	δ_{yz}	R_z^{max}
HF ($d = 0.9b_0$), σ_{HF}	1.074	-0.305	0.148	-0.386
HF ($d = 1.0b_0$), σ_{HF}	1.067	-0.298	0.108	-0.384
HF ($d = 1.5b_0$), σ_{HF}	1.051	-0.283	0.027	-0.381
HF ($d = 2.0b_0$), σ_{HF}	1.047	-0.279	0.010	-0.381
HF (no complex), σ_{HF}	1.045	-0.277	0.000	- - -
$MeNH_2$ ($d = 0.9b_0$), n_N	0.771	0.241	0.080	-0.439
$MeNH_2$ ($d = 1.0b_0$), n_N	0.759	0.248	0.067	-0.566
$MeNH_2$ ($d = 1.5b_0$), n_N	0.751	0.262	0.035	-0.837
$MeNH_2$ ($d = 2.0b_0$), n_N	0.755	0.265	0.013	-0.756
$MeNH_2$ (no complex), n_N	0.759	0.268	0.000	- - -

centre-of-mass away from the nitrogen atom resulting in the observed depletions in the extracule density in this area. This observed migration of electrons from the hydrogen to the fluorine in the H-F bond combined with the donation of electrons from nitrogen to the electron deficient hydrogen is in excellent agreement with the resonance-covalency[54,55] interpretation of hydrogen bonding (or any non-covalent interaction) as opposed to the more traditional dipole-dipole interaction interpretation.

To *quantify* the differences between the extracule densities of σ_{HF} and n_N before and after complexation, we have employed similar measures as noted previously including the zeroth moment $\langle R_{yz}^0 \rangle$ of $E_d^{\sigma_{HF},\text{HF-MeNH}_2}(0,R_y,R_z)$ and $E_d^{n_N,\text{HF-MeNH}_2}(0,R_y,R_z)$ as well as R_z^{max} of both the extracules and the extracule deformation densities. For $\Delta E_d^{\phi}(0,R_y,R_z)$, we also define a new measure, δ_{yz}, referring to the magnitude of the difference between the extracules:

$$\delta_{yz} = \int_{-\infty}^{\infty}\int_{-\infty}^{\infty} \left|\Delta E_d^{\phi}(0,R_y,R_z)\right| \mathrm{d}R_y\,\mathrm{d}R_z \qquad (22)$$

These metrics are all listed in Table 5. As before, the introduction of an electronegative species (N in $MeNH_2$) caused an increase in $\langle R_{yz}^0 \rangle$ for the HF bond LMO. This effect is even present in the case where $d = 2.0b_0$; it is small, but still significant. However, no trend is apparent in the zeroth moment for the lone pair. When observing the position of the maxima, as noted in the discussion of Figure 4, the maxima shift toward the F atom for the HF bond, while they shift away from the nitrogen atom, towards the acceptor species (HF) in the case of the $MeNH_2$ lone pair.

δ_{yz} provides us with an absolute measure of the variation in the extracule density for each LMO as a function of the intermolecular interaction. It is relatively large when $d = 0.9b_0$ ($S = 0.148$ and $S = 0.080$ for σ_{HF} and n_N, respectively) and decreases as the methylamine and hydrogen fluoride are separated. At $d = 2.0b_0$, δ_{yz} reduces to 0.010 (σ_{HF}) and 0.013 (n_N) suggesting that the strength of the hydrogen bonding interaction is related to δ_{yz}. Observing these changes in δ_{yz} can provide an indication of the strength of the interaction between the donor and acceptor species, especially when weighted against the energetic cost of nuclear repulsion with decreasing d. Further work to elucidate relationships between intermolecular interaction energies and electron pair distributions (intracular and/or extracular) in position and momentum spaces is ongoing in our laboratory.

4 Conclusions

Herein, we have introduced a novel tool for the analysis of electronic structure. While the extracule density has been studied in the past, the breadth of systems studied has been very limited. This could be due in part to the complexity involved in interpreting a probability density for $N(N-1)/2$ pairs of electrons. By accessing localized regions of chemical space through the use of ER localized molecular orbitals, we not only simplify the interpretation of the extracule density, but also afford a quantum mechanical interpretation of "chemically intuitive" features of electronic structure.

While this study only involved calculations performed at the HF level of theory, the general trends in chemical behaviour observed are not expected to change through the use of correlated models. Regardless, the localized pair model does offer the capability to perform analyses using Kohn-Sham orbitals to account for correlation.[40] Studies are presently underway in our lab detailing the effects of correlation within localized chemical bonds for intracule densities and could easily be implemented for the study of extracule densities.

This study has demonstrated the types of information that can be extracted from the localized extracule density for simple systems, but one can extend these calculations to larger systems. The main obstacle to the study of large chemical systems is the time required for such calculations. However, through the use of LMOs, this barrier can be partially overcome by the inclusion of only atomic orbitals in close proximity to the molecular orbital under scrutiny. While this study was conducted with ER LMOs, one can apply the technique in an identical fashion to other localized orbitals, such as the previously mentioned NBOs, IBOs, and ALMOs, as well as any canonical molecular orbital of interest.

5 Acknowledgements

The authors acknowledge the Natural Sciences and Engineering Research Council of Canada, the Canadian Foundation for Innovation (CFI) and the University of Prince Edward Island for the financial support that made this research possible. The authors also thank Dr. Ajit Thakkar for insight regarding the calculation of the extracule densities. Computational resources were provided by ACENET, the regional high performance computing consortium for universities in Atlantic Canada. ACENET is funded by CFI, the Atlantic Canada Opportunities Agency (ACOA), and the provinces of Newfoundland and Labrador, Nova Scotia, and New Brunswick.

References

1 E. Schrödinger, *Ann. Phys.*, 1926, **79**, 361.
2 P. Hohenberg and W. Kohn, *Phys. Rev.*, 1964, **136**, B864.
3 C. A. Coulson and A. H. Neilson, *Proc. Phys. Soc. London*, 1961, **78**, 831.
4 A. J. Proud and J. K. Pearson, *J. Chem. Phys.*, 2010, **133**, 134113.
5 A. J. Thakkar and N. J. Moore, *Int. J. Quantum Chem.*, 1981, **20**, 393–400.

6 A. Thakkar, *Density Matrices and Density Functionals*, Reidel, Dordrecht, 1987, pp. 553–581.
7 A. J. Coleman, *Int. J. Quantum Chem.*, 1967, **1**, 457.
8 C. Sarasola, J. M. Ugalde and R. J. Boyd, *J. Phys. B: At. Mol. Opt. Phys.*, 1990, **23**, 1095.
9 L. Dominguez, M. Aguado, C. Sarasola and J. M. Ugalde, *J. Phys. B: At. Mol. Opt. Phys.*, 1992, **25**, 1137.
10 J. Wang, A. N. Tripathi and V. H. S. Jr, *J. Phys. B: At. Mol. Opt. Phys.*, 1993, **26**, 205.
11 T. Koga, H. Matsuyama, E. Romera and J. S. Dehesa, *Phys. Rev. A*, 1998, **57**, 4212.
12 T. Koga and H. Matsuyama, *J. Chem. Phys.*, 1998, **108**, 3424.
13 F. J. Galvez, E. Buendia and A. Sarsa, *J. Chem. Phys.*, 1999, **111**, 3319.
14 T. Koga, H. Matsuyama, J. M. Molina and J. S. Dehesa, *Eur. Phys. J. D*, 1999, **7**, 17.
15 T. Koga, H. Matsuyama, J. S. Dehesa and A. J. Thakkar, *J. Chem. Phys.*, 1999, **110**, 5763.
16 H. Matsuyama and T. Koga, *Chem. Phys. Lett.*, 1999, **300**, 515.
17 S. P. McCarthy and A. J. Thakkar, *Int. J. Quantum Chem.*, 2011, **111**, 753.
18 Z. A. M. Zielinski and J. K. Pearson, *Comp. Theor. Chem.*, 2013, **1003**, 79–90.
19 D. C. Hennessey, B. J. H. Sheppard, D. E. C. K. Mackenzie and J. K. Pearson, *Phys. Chem. Chem. Phys.*, 2014, **16**, 25548.
20 J. E. Lennard-Jones and J. A. Pople, *Proc. Roy. Soc. (London)*, 1950, **A202**, 166.
21 J. E. Lennard-Jones and J. A. Pople, *Proc. Roy. Soc. (London)*, 1950, **A210**, 190.
22 J. Foster and S. Boys, *Rev. Mod. Phys.*, 1960, **32**, 300–302.
23 C. Edmiston and K. Ruedenberg, *Rev. Mod. Phys.*, 1963, **35**, 457–464.
24 J. Pipek and P. Mezey, *J. Chem. Phys.*, 1989, **90**, 4916–4926.
25 W. J. V. Niessen, *J. Chem. Phys.*, 56, **1972**, 4290.
26 J. P. Foster and F. Weinhold, *J. Am. Chem. Soc.*, 1980, **102**, 7211–7218.
27 A. E. Reed, L. A. Curtiss and F. Weinhold, *Chem. Rev.*, 1988, **88**, 899–926.
28 F. Weinhold and J. E. Carpenter, *The Structure of Small Molecules and Ions*, Plenum, New York, 1988, pp. 227–236.
29 E. D. Glendening, C. R. Landis and F. Weinhold, *WIREs Comput. Mol. Sci.*, 2012, **2**, 1–42.
30 F. Weinhold, *J. Comp. Chem.*, 2012, **33**, 2363–2379.
31 G. Knizia, *J. Chem. Theory Comput.*, 2013, **9**, 4834.
32 G. Knizia and J. E. M. N. Klein, *Angew. Chem. Int. Ed.*, 2015, **54**, 1.
33 H. Stoll, G. Wagenblast and H. Preuss, *Theor. Chem. Acta*, 1980, **57**, 169–178.
34 J. M. Cullen, *Int. J. Quantum Chem., Quantum Chem. Symp.*, 1991, **25**, 193–212.
35 E. Gianinetti, M. Raimondi and E. Tornaghi, *Int. J. Quantum Chem.*, 1996, **60**, 157–166.
36 T. Nagata, O. Takahashi, K. Saito and S. Iwata, *J. Chem. Phys.*, 2001, **115**, 3553–3560.
37 R. Z. Khaliullin, E. A. Cobar, R. C. Lochan, A. T. Bell and M. Head-Gordon, *J. Phys. Chem. A*, 2007, **111**, 8753–8765.
38 R. Z. Khaliullin, M. Head-Gordon and A. T. Bell, *J. Chem. Phys.*, 2006, **124**, 204105.
39 M. Mura and P. Knowles, *J. Chem. Phys.*, 1996, **104**, 9848–9858.
40 W. Kohn and L. J. Sham, *Phys. Rev.*, 1965, **140**, A1133.
41 M. W. Schmidt, K. K. Baldridge, J. A. Boatz, S. T. Elbery, M. S. Gordon, J. H. Jensen, S. Koseki, N. Matsunaga, K. A. Nguyen, S. J. Su, T. L. Windus, M. Dupuis and J. A. Montgomery, *J. Comput. Chem.*, 1993, **14**, 1347–1363.
42 Wolfram Research, Inc., *Mathematica 8*, 2010.
43 P. G. Mahaffy, B. Bucat, R. Tasker, J. C. Kotz, P. M. Treichel, G. C. Weaver and J. McMurry, *Chemistry: Human Activity, Chemical Ractivity*, Nelson Education, Ltd., Toronto, 1st edn, 2011.
44 P. Y. Bruice, *Organic Chemistry*, Pearson Education, Inc., New Jersey, 7th edn, 2012.
45 T. Koga and H. Matsuyama, *J. Phys. B: At. Mol. Opt. Phys.*, 1997, **30**, 5631.
46 T. Koga, *J. Chem. Phys.*, 1998, **108**, 2515.
47 J. M. Mercero, J. Fowler, C. Sarasola and J. M. Ugalde, *Phys. Rev. A*, 1999, **59**, 4255.
48 E. Valderrama, X. Fradera and J. M. Ugalde, *J. Chem. Phys.*, 2001, **115**, 1987.
49 E. Valderrama, J. M. Mercero and J. M. Ugalde, *J. Phys. B: At. Mol. Opt. Phys.*, 2001, **34**, 275.
50 A. de Meijere, *Angew. Chem. Int. Ed.*, 1979, **18**, 809–826.
51 C. A. Coulson and W. E. Moffitt, *Phil. Mag.*, 1949, **40**, 1.
52 W. A. Bernett, *J. Chem. Educ.*, 1967, **44**, 17.
53 J. Řezáč, K. E. Riley and P. Hobza, *J. Chem. Theory Comput.*, 2011, **7**, 2427.
54 F. Weinhold and R. A. Klein, *Mol. Phys.*, 2012, **110**, 565.
55 F. Weinhold and R. A. Klein, *Chem. Educ. Res. Pract.*, 2014, **15**, 276.